Localised High Resolution Spectral Estimator for Resolving Superimposed Peaks in NMR Signals

Shanglin Ye[a,*], Elias Aboutanios[a], Donald S. Thomas[b], James M. Hook[b]

[a]*School of Electrical Engineering and Telecommunications, University of New South Wales, Sydney, NSW 2052, Australia*
[b]*NMR Facility, Mark Wainwright Analytical Centre, University of New South Wales, Sydney, NSW 2052, Australia*

Abstract

Nuclear magnetic resonance (NMR) spectroscopy is the prime technique for studying molecular and biomolecular structure as well as dynamics. The time domain NMR signal can be ideally modelled as the sum of damped complex exponentials in additive Gaussian noise. The spectrum of the signal may contain regions having overlapping peaks. In order to understand the underlying chemical structure, these peaks need to be detected and resolved. In this paper, we propose the Localised Capon Estimator (LoCapE) for resolving closely spaced peaks in the NMR spectrum when the actual number of peaks is unknown. The novel method is able to efficiently retrieve the correct number of components and obtain high resolution spectral estimates in the selected regions of the spectrum. LoCapE is tested with simulated and actual proton NMR spectra to verify its performance.

Keywords: Capon; spectral estimation; peak detection; nuclear magnetic resonance spectroscopy; coupling constant.

1. Introduction

Nuclear magnetic resonance (NMR) spectroscopy is a powerful tool for the study of molecular and biomolecular structure and dynamics, [1, 2]. The acquired discrete time domain signal obtained from the NMR spectrometer, which is referred to as the free induction decay (FID), can

*Corresponding author. TEL: +61 2 9385 4803 (S. Ye). *E-mail addresses:* shanglin.ye@unsw.edu.au (S. Ye), elias@ieee.org (E. Aboutanios), donald.thomas@unsw.edu.au (D. S. Thomas), j.hook@unsw.edu.au (J. M. Hook).

be ideally modelled as a sum of a number of decaying complex exponentials in additive noise [3],

$$x(n) = \sum_{i=1}^{I} a_i e^{j\phi_i} e^{(-\eta_i + j2\pi f_i)n} + w(n). \tag{1}$$

In Eq. (1), we have $n = 0 \ldots N-1$. I is the number of components in the signal and is usually unknown in practice. The parameters a_i, ϕ_i, f_i and η_i are respectively the absolute amplitude, the initial phase, the frequency and the damping factor of the i^{th} component. The noise terms $w(n)$ are assumed to be additive Gaussian noise with zero mean and variance σ^2.

In practice, the spectrum of the FID usually contains heavily overlapped peaks – that is the frequencies of different components are close to each other. In order to understand the underlying structure of the chemical sample being tested, these overlapping peaks need to be resolved. In practice, however, due to lineshape distortion caused by experimental artefacts such as magnetic field inhomogeneities, the experimental NMR datasets usually deviate from the ideal model. At the same time, the number of components I is unknown and the number of data points N is often very large ($N \geq 2^{14}$). These limitations make the spectral estimation task quite challenging.

There is a wealth of literature on spectral estimation algorithms that can be applied to NMR signals to improve on the resolution of the spectrum. These may be classed into two main kinds: parametric estimators and non-parametric estimators. When dealing with spectral estimation for long FIDs with an unknown number of overlapping components, as is the case for NMR, traditional high resolution parametric estimators, such as MUSIC [4], ESPRIT [5, 6] and Matrix Pencil [7], are not desirable as they require the component number to be known *a priori*. They are also computationally heavy for estimating the parameters of the whole spectrum because of the singular value decomposition (SVD). The Information Theoretic Matrix Pencil Method (ITMPM) [8], combines information theory criteria, such as the Akaike criteria (AIC) [9] or minimum description length (MDL) [10] with a high resolution parametric estimator to find the number of components in the estimation process. Nonetheless, heavy computational cost still make the algorithm undesirable. Frequency-selective estimators [11] have been proposed for reducing the computational cost of parametric estimators by selecting spectrum regions of interest. However, they cannot deal with the detection of numbers of components.

Non-parametric estimators including the Capon spectral estimator [12], the amplitude and

phase estimator (APES) [13] and the recent Iterative Adaptive Approach (IAA) [14], alongside with the damped versions [15], on the other hand, do not need the *a priori* information of the number of signal components. They rely on the design of adaptive finite impulse response (FIR) filter-banks, with each filter tuned to one of the frequency bins of interest, by solving certain constrained minimisations. However, these methods require the estimation of the covariance matrix of the signal, which results in a trade-off between the achievable resolution and smoothness of the spectrum, [16]. Furthermore, the estimated covariance matrix must be inverted, which also causes computational difficulties. Consequently, the achievable resolution of the estimated spectrum in the case of large N is limited by these two problems. More recently, compressed sensing (CS) techniques [17, 18, 19], as spectral analysis approaches, have been modified and applied to the processing of NMR signals, especially for non-uniformly sampled datasets with the aim of reducing the data acquisition and hence experiment time particular in multi-dimensional experiments [20]. However, the drawbacks of CS approaches are those of computational cost and performance on noisy data. CS techniques generally require a dictionary, and as NMR data involves distorted lines that deviate from ideal signal models, this necessitates the measurement of signal templates [21], which can be a significant burden. In addition, the off-grid problem remains a challenge.

In this paper, we present a novel high resolution spectral estimator that is capable of efficiently separating closely overlapped peaks in a specific region in NMR spectroscopy when the number of components in the region is not given (in which case the parametric high resolution methods are not implementable). We develop a localised version of the non-parametric damped Capon estimator [15], which we call the Localised Capon Estimator (LoCapE). The undamped version has previously been developed in [22]. This spectral estimator not only achieves a high resolution, but also exhibits low computational complexity. Thus, it can be efficiently implemented for NMR data processing as a "zooming" operator on user-defined spectral regions to resolve overlapping peaks. We evaluate the estimator on both simulated undamped/damped exponential signals and experimental ^{1}H NMR datasets that contain heavily overlapped peaks. It is important to note that this algorithm is applicable in areas other than NMR where the damped exponential model holds. These include, mechanical systems, radar, sonar, etc...

The structure of the paper is organised as follows. In the following section, we present the

detailed derivation of LoCapE with its efficient implementation left for the appendix. In Section 3, we show the evaluation results of the estimator, which include the results on simulated exponential signals and experimental ^{1}H datasets of codeine. Finally, some conclusions are drawn in Section 4.

2. The Estimation Algorithm

2.1. Notation

In the rest of the paper, we use lower case and upper case bold characters, such as $\mathbf{x}$ and $\mathbf{X}$, to represent vectors and matrices respectively. The asterisk, *, is used to denote the conjugate of a complex number. For a matrix $\mathbf{A}$ (equally for a vector), $\mathbf{A}^T$ stands for its transpose and $\mathbf{A}^H$ stands for its conjugate transpose. Also, $\hat{\lambda}$ stands for the estimated value of parameter λ. Finally, we use $\lceil\lambda\rceil$ and $\lfloor\lambda\rfloor$ to respectively represent the ceiling and floor operations of λ.

2.2. The Damped Capon Estimator

For the clarity of presentation, before putting forward the localised version, we briefly review the original damped Capon which is presented in [15]. Given a length-N signal $x(n)$ ideally modelled as Eq. (1), the goal of the damped Capon estimator is to design a length-M ($M < N$) adaptive filter $\mathbf{h}(f, \eta)$ at frequency f and damping factor η that minimises the power of the output signal, subject to the output of a damped exponential at f and η be constraint to 1. Now let $\mathbf{x}_l = [x(l-1), x(l), \dots x(N-L-l)]^T$. The minimisation problem can be expressed as

$$\min_{\mathbf{h}} \sum_{l=1}^{L} |\mathbf{h}^H(f,\eta)\mathbf{x}_l|^2 \quad \text{s.t.} \quad \mathbf{h}^H(f,\eta)\mathbf{s}_M(f,\eta) = 1, \tag{2}$$

where

$$\mathbf{s}_m(f,\eta) = [1, e^{-j2\pi f}, \dots, e^{(-\eta - j2\pi f)(m-1)}]^T, \tag{3}$$

is the damped Fourier template vector of length m.

Let $\mathbf{X}$ be the $M \times L$ ($L = N - M + 1$ and $M < L$) Hankel matrix of the signal

$$\mathbf{X} = \begin{bmatrix} x(0) & x(1) & \cdots & x(L-1) \\ x(1) & x(2) & \cdots & x(L) \\ \vdots & \vdots & \ddots & \vdots \\ x(M-1) & x(M) & \cdots & x(N-1) \end{bmatrix}, \tag{4}$$

and $\mathbf{R}$ be the estimate of the signal covariance. The solution of the minimisation problem results in the damped Capon spectral estimate at frequency f and damping factor η given by [15]:

$$\hat{a}_{\text{Capon}}(f,\eta) = \frac{\mathbf{s}_M^H(f,\eta)\mathbf{R}^{-1}\mathbf{X}\mathbf{s}_L^*(f,\eta)}{L_\eta \mathbf{s}_M^H(f,\eta)\mathbf{R}^{-1}\mathbf{s}_M(f,\eta)},\ f \in [-0.5, 0.5], \eta \in \mathbf{\Gamma}, \tag{5}$$

where $\mathbf{\Gamma} = [\eta(1), \eta(2), \ldots]^T$ is the pre-defined damping factor grid and

$$L_\eta = \sum_{n=0}^{L-1} e^{-2\eta n}. \tag{6}$$

In Eq. (5), $\mathbf{R}$ can be obtained by the forward-only estimation,

$$\mathbf{R} = \mathbf{R}_{\text{F}} = \mathbf{X}\mathbf{X}^H, \tag{7}$$

or the forward-backward averaged estimation,

$$\mathbf{R} = \mathbf{R}_{\text{FB}} = \frac{1}{2}\left(\mathbf{X}\mathbf{X}^H + \tilde{\mathbf{X}}\tilde{\mathbf{X}}^H\right), \tag{8}$$

where $\tilde{\mathbf{X}}$ is the $M \times L$ Hankel matrix of the complex conjugate time-reversed signal,

$$\tilde{\mathbf{X}} = \begin{bmatrix} x^*(N-1) & x^*(N-2) & \cdots & x^*(N-L) \\ x^*(N-2) & x^*(N-3) & \cdots & x^*(N-L-1) \\ \vdots & \vdots & \ddots & \vdots \\ x^*(N-M) & x^*(N-M-1) & \cdots & x^*(0) \end{bmatrix}. \tag{9}$$

One may consider that using the forward-only covariance matrix, Eq. (7) returns higher resolution of the estimator than the backward-forward covariance matrix Eq. (8) [23]. However, this is only true when the filter length M is relatively small. As M approaches the smoothing length L, the resolution of the forward-backward Capon becomes higher than the forward-only Capon.

2.3. The Localised Capon Estimator

It is well-known that the resolution of the Capon estimator improves as the filter length M increases [13, 24], however achieved at the expense of less averaging (dictated by $L = N - M + 1$) giving a less smooth spectrum. In order to obtain a non-singular (invertible) covariance matrix $\mathbf{R}$, the number of samples being averaged must be strictly larger than the number of degrees of freedom, that is $M < L$. Therefore, for any fixed N, the original algorithm is subject to a limit on the achievable resolution of the spectrum estimation. Also, inverting the $M \times L$ covariance matrix $\mathbf{R}$ is computationally expensive, especially for large N (that is long FIDs). To overcome these limitations, we propose the localised version of the algorithm, LoCapE that permits us to relax the averaging requirement in order to improve the resolution, as well as significantly reduce the computational burden.

Let us start by assuming that the frequency grid of interest is the whole spectrum with each bin separated by $1/M$: $\mathbf{f} = M^{-1}[0, 1, 2, \ldots, (M-1)]^T$. Define $\mathbf{F}$ as the $M \times M$ unitary Fourier matrix scaled by $\sqrt{M}$:

$$\mathbf{F} = \begin{bmatrix} 1 & 1 & \cdots & 1 \\ 1 & e^{j\frac{2\pi}{M}} & \cdots & e^{j\frac{2\pi(M-1)}{M}} \\ \vdots & \vdots & \ddots & \vdots \\ 1 & e^{j\frac{2\pi(M-1)}{M}} & \cdots & e^{j\frac{2\pi(M-1)^2}{M}} \end{bmatrix}. \tag{10}$$

Notice that $\mathbf{s}_M(f, 0)$, where $f \in \mathbf{f}$, is one of the columns of $\mathbf{F}$. Eq. (5) can then be re-written as

$$\begin{aligned} \hat{a}_{\text{Capon}}(f, \eta) &= \frac{\mathbf{s}_M^H(f,\eta)\mathbf{F}\mathbf{F}^H\mathbf{R}^{-1}\mathbf{F}\mathbf{F}^H\mathbf{X}\mathbf{s}_L^*(f,\eta)}{L_\eta \mathbf{s}_M^H(f,\eta)\mathbf{F}\mathbf{F}^H\mathbf{R}^{-1}\mathbf{F}\mathbf{F}^H\mathbf{s}_M(f,\eta)} \\ &= \frac{\left[\mathbf{F}^H\mathbf{s}_M(f,\eta)\right]^H \left(\mathbf{F}^H\mathbf{R}\mathbf{F}\right)^{-1} \mathbf{F}^H\mathbf{X}\mathbf{s}_L^*(f,\eta)}{L_\eta \left[\mathbf{F}^H\mathbf{s}_M(f,\eta)\right]^H \left(\mathbf{F}^H\mathbf{R}\mathbf{F}\right)^{-1} \mathbf{F}^H\mathbf{s}_M(f,\eta)}. \end{aligned} \tag{11}$$

Now it is clear that $\mathbf{F}^H\mathbf{s}_M(f, \eta)$ is the discrete Fourier transform of $\mathbf{s}_M(f, \eta)$ and most of the energy of $\mathbf{s}_M(f, \eta)$ is concentrated in a few elements in the neighbourhood of the element corresponding to the column index of f. Therefore, we propose reducing the dimensionality of the problem localising the Fourier matrix $\mathbf{F}$ to a matrix $\bar{\mathbf{F}}$ consisting of only a few column vectors, specifically $r \ll M$ vectors, around $\mathbf{s}_M(f, \eta)$. In the following, we use the overbar to refer to the dimensionality-

reduced quantities. Then

$$\bar{\mathbf{s}}_r(f,\eta) = \bar{\mathbf{F}}^H \mathbf{s}_M(f,\eta), \tag{12}$$

is a length-r vector that has L_η for the entry corresponding to f. Clearly the localised algorithm reverts to the original if we put $r = M$.

When the frequency grid of interest is denser than $\mathbf{f}$, $\mathbf{F}$ is no longer a unitary matrix. Nevertheless, the fact that most of the energy of $\mathbf{F}^H\mathbf{s}_M(f,\eta)$ is concentrated in a small number of points in the neighbourhood of the frequency of interest f still holds. Now, let the desired sampling grid of the spectrum be of size $N_f \geq M$. Then the frequency bins in the spectrum separated by $1/N_f$ and $\mathbf{F}$ is a $N_f \times N_f$ matrix. In this case, we can construct the localised Fourier matrix $\bar{\mathbf{F}}$ to have the centre column corresponding to the desired frequency, f, and p columns either side of f spaced by $q = \lfloor N_f/M \rfloor$ bins,

$$\bar{\mathbf{F}} = \begin{bmatrix} 1 & \cdots & 1 & 1 & 1 & \cdots & 1 \\ e^{j2\pi(f-\frac{pq}{N_f})} & \cdots & e^{j2\pi(f-\frac{q}{N_f})} & e^{j2\pi f} & e^{j2\pi(f+\frac{q}{N_f})} & \cdots & e^{j2\pi(f+\frac{pq}{N_f})} \\ \vdots & & \vdots & \vdots & \vdots & & \vdots \\ e^{j2\pi(f-\frac{pq}{N_f})(M-1)} & \cdots & e^{j2\pi(f-\frac{q}{N_f})(M-1)} & e^{j2\pi f(M-1)} & e^{j2\pi(f+\frac{q}{N_f})(M-1)} & \cdots & e^{j2\pi(f+\frac{pq}{N_f})(M-1)} \end{bmatrix}. \tag{13}$$

Now let $\bar{\mathbf{X}} = \bar{\mathbf{F}}^H\mathbf{X}$ and $\bar{\tilde{\mathbf{X}}} = \bar{\mathbf{F}}^H\tilde{\mathbf{X}}$ be the localised Fourier-transformed Hankel signal matrices, the localised Fourier-transformed forward-backward averaged covariance matrix becomes

$$\bar{\mathbf{R}} = \bar{\mathbf{F}}^H\mathbf{R}_{\mathrm{FB}}\bar{\mathbf{F}} = \frac{1}{2}\left(\bar{\mathbf{X}}\bar{\mathbf{X}}^H + \bar{\tilde{\mathbf{X}}}\bar{\tilde{\mathbf{X}}}^H\right). \tag{14}$$

This leads to the amplitude spectrum estimate at frequency f and damping factor η being

$$\hat{a}_{\mathrm{LoCapE}}(f,\eta) = \frac{\bar{\mathbf{s}}_r^H(f,\eta)\bar{\mathbf{R}}^{-1}\bar{\mathbf{X}}\mathbf{s}_L^*(f,\eta)}{L_\eta\bar{\mathbf{s}}_r^H(f,\eta)\bar{\mathbf{R}}^{-1}\bar{\mathbf{s}}_r(f,\eta)}. \tag{15}$$

The estimate obtained by Eq. (15) shows peaks at $[\hat{f}_i, \hat{\eta}_i]$, $i = 1 \ldots I$. Similar to the approach given in [15], we propose that the final 1-D amplitude spectrum estimate with respect to f is obtained by the maximiser along the damping factor axis,

$$\hat{a}_{\mathrm{LoCapE}}(f) = \max_{\eta\in\boldsymbol{\Gamma}} \left\{ \frac{\bar{\mathbf{s}}_r^H(f,\eta)\bar{\mathbf{R}}^{-1}\bar{\mathbf{X}}\mathbf{s}_L^*(f,\eta)}{L_\eta\bar{\mathbf{s}}_r^H(f,\eta)\bar{\mathbf{R}}^{-1}\bar{\mathbf{s}}_r(f,\eta)} \right\}. \tag{16}$$

Clearly when $\boldsymbol{\Gamma} = [0]$, LoCapE becomes the undamped version [22].

The application of Eq. (15) for each frequency bin of interest involves operations on small size matrices, which significantly reduces the dimensionality of the original algorithm. Furthermore, as the covariance matrix is of size $r \times r$, an L that is smaller than $\lfloor N/2 + 1 \rfloor$ is required for it to be invertible. This reduced requirement on the amount of smoothing allows us to reduce L giving a corresponding increase in M (for a fixed N) and consequently a significant improvement in the spectral resolution with respect to the original algorithm.

Finally, we summarise the spectral estimation procedure as follows:

1. Define the LoCapE filter length M, where $M > \lceil N/2 \rceil$, and set the corresponding smoothing length $L = N - M + 1$. Partition the signal to the $M \times L$ Hankel matrices $\mathbf{X}$ and $\tilde{\mathbf{X}}$ as shown in Eqs. (4) and (9).
2. Set the length of the localised region $r = 2p + 1$, with p being a very small integer (e.g. $1, 2, 3...$), selected according to the broadness of the peaks in the DFT spectrum. Also set N_f be the desired sampling density of the estimated spectrum.
3. Define the frequency grid $\mathbf{f} = [f(1), f(2), \dots f(n_f)]^T$ for the region of interest in the spectrum (that is the region that is suspected of containing overlapping peaks). Generally we have that $n_f \ll N_f$.
4. Define the damping factor grid $\mathbf{\Gamma} = [\eta(1), \eta(2), \dots, \eta(n_\eta)]$ such that for the components that $f_i \in \mathbf{f}$, $\eta(1) < \eta_i < \eta(n_\eta)$ (that the damping factors of all the signal components in the spectrum region of interest are in the grid).
5. For each $f \in \mathbf{f}$ and $\eta \in \mathbf{\Gamma}$, do:
   (a) Construct the localised Fourier matrix $\bar{\mathbf{F}}$ of size $M \times r$ by Eq. (13), the Fourier template vectors $\mathbf{s}_M(f, \eta)$, $\mathbf{s}_L(f, \eta)$ by Eq. (3) and then the localised Fourier vector $\bar{\mathbf{s}}_r(f, \eta)$ by Eq. (12);
   (b) Using the efficient method presented in Appendix A, calculate the Fourier-transformed localised Hankel matrices $\bar{\mathbf{X}}$ and $\bar{\tilde{\mathbf{X}}}$, and then get the Fourier-transformed localised covariance matrix by Eq. (14);
   (c) Obtain the 2-D spectrum estimation at frequency f and damping factor η by Eq. (11).
6. Finally, find the 1-D spectrum estimation using Eq. (16).

3. Results

In this section we verify the ability of LoCapE to detect closely spaced peaks in NMR spectra. We present results using simulated exponentials and two experimental ^{1}H NMR datasets. For both simulated and experimental results, we are only interested in the comparison of the ability of various algorithms for peak separation and frequency estimation, and the comparison of amplitude estimation is beyond the scope of this paper.

3.1. Simulation Results

We first apply the localised algorithm to a simulated exponential signal containing two closely spaced components. Consider the signal

$$x(n) = e^{(-\eta+j2\pi f_1)n} + e^{j\theta}e^{(-\eta+j2\pi f_2)n} + w(n), \quad n = 0 \dots N-1, \tag{17}$$

where $N = 64$ is the signal length, η is the damping factor and $f_1, f_2 \in [0, 1]$ are the normalised frequencies. In the simulations, we fix the SNR to $\rho = \sigma^{-2} = 25$dB, set $f_1 = 0.5$ and vary f_2 from 0.485 to 0.499. θ is assumed to be uniformly distributed over $[0, 2\pi]$ and is randomly selected in each Monte Carlo run.

We compare the capability of LoCapE to resolve the two peaks with the original Capon [12], ITMPM [8] and MUSIC [4]. Notice that among the methods, MUSIC requires the number of components *a priori*. For LoCapE, we set the localised region to $r = 5$ and vary the smoothing length L. We also use a spectral sampling density $N_f = 128N$. For the original Capon, we obtain the highest resolution by setting the filter length to $M' = N/2 = 32$, which is identical to the the matrix pencil parameter of ITMPM and the degree of freedom used in MUSIC. We report results using both information criteria schemes in ITMPM for detecting the number of components.

In assessing the algorithms' performance, two closely spaced peaks are considered to be resolved in the case of MUSIC and LoCapE if the following rule is satisfied [25]:

$$\epsilon = 2\hat{a}(f_\mathrm{m}) - \hat{a}(f_1) - \hat{a}(f_2) < 0 \tag{18}$$

where $\hat{a}(f)$ is the spectrum estimation at frequency f, and $f_\mathrm{m} = 0.5(f_1 + f_2)$, which is the intermediate frequency between f_1 and f_2. As for ITMPM, which finds the number of components

and the corresponding parameters instead of producing spectral estimates, we consider the two components to be resolved when the estimated number of components is two.

Figure 1 shows the rate of successfully resolving both peaks as a function of f_2 when $\eta = 0$. The results show that as L becomes smaller, LoCapE has better ability to separate the two peaks. When $L = 20$, it outperforms all the other methods including the state-of-art high resolution MUSIC, without knowing the actual number of components. Also, notice that the ITMPM-AIC always has a success rate less than 100% (approximately 98% in this case). The results clearly show that the proposed estimator exhibits the best ability to separate closely spaced exponentials. Figures 2 and 3 show the resolving power of various methods when $\eta = 0.03$ and $\eta = 0.05$, where LoCapE shows similar behaviour while the performance of ITMPM and MUSIC deteriorates significantly.

Then we examine the accuracy of frequency estimation of LoCapE. In this simulation, we set in Eq. (17) $f_1 = 0.5$ and $f_2 = 0.48$. θ were randomly chosen in each run. We obtain the frequency estimates of LoCapE by peak picking in the estimated amplitude spectra. The parameters of LoCapE and Capon are the same as the previous test. Figures 4 and 5 show the root mean square error (RMSE) of the estimates of f_1 versus SNR when $\eta = 0$ and $\eta = 0.05$ respectively. For comparison, we also show the CRLB [26], the results of original Capon estimator, ESPRIT [5, 6] and ITMPM. For ESPRIT, the degree of freedom length is set to $M' = N/2$, which is identical to the pencil parameter for ITMPM. $I = 2$ is given both ESPRIT and ITMPM as *a priori* information, and we also show the result when we use MDL to determine the number of components in ITMPM. It can be clearly found in Figure 4 that the RMSE of all the estimators are similar at high SNR and follow the trend of the CRLB, with LoCapE having the lowest breakdown threshold. ESPRIT and ITMPM share similar performance, but for ITMPM, when I is unknown and determined by MDL, the breakdown threshold is higher than the case when I is given. We know that smaller L leads to a less smoothed spectrum estimation. Therefore, the RMSE of LoCapE when $L = 20$ is marginally larger, and it becomes closer to both CRLB and the original Capon as L approaches $N/2$. The result illustrates that LoCapE is capable of achieving frequency estimates that is comparable to the parametric estimators without knowing the number of components. This also illustrates the trade-off that exists between the resolution and the RMSE. Before moving onto the next experiment, we note that although related figures are not shown in this paper, we have tested the resolving power

and estimation accuracy of LoCapE on signals with different N, where we obtained consistent performance.

Next, we apply LoCapE to a simulated NMR signal consisting of six damped complex exponentials according to the model given in Eq. (1). We set $N = 2,048$ and ϕ_i to be zero for all i. The amplitudes, frequencies and damping factors are listed in Table 1. The signal components are chosen so that components 2 and 3 are very close to each other. Component 4, 5 and 6 are closely spaced as well with one of them (component No. 4) being more damped than the other two. The smoothing length of LoCapE that we employ in this example is $L = \lfloor N/2 \rfloor$, and we set the size of the localised region $r = 7$. We use $N_f = 16N$ points in the spectral estimation and apply the localised algorithm to the selected regions of $\mathbf{f}_1 = [0.497, 0.505]$ and $\mathbf{f}_2 = [0.69, 0.71]$ with a damping factor grid of $\mathbf{\Gamma} = [0.005, 0.02]$. We compare the performance with N_f-point DFT and ITMPM, with the latter implemented using both detection schemes a pencil parameter $L' = N/2$.

Figure 6 shows the success rate for simultaneously resolving two sets of components $\{2, 3\}$, and $\{4, 5, 6\}$ versus SNR for LoCapE, DFT and ITMPM. We see from the figure that LoCapE is still capable of resolving the components down to a lower SNR than the other algorithms. Note that although ITMPM - AIC operates down to a lower SNR than the ITMPM - MDL, its success rate never reaches 100% even for high SNR. On the other hand, the DFT cannot resolve the components at any SNR.

In order to clearly demonstrate how LoCapE performs in the selected regions of interest, we include in Figure 7 the "zoomed in" spectra around $f = 0.5$ and $f = 0.7$. In each selected region, we show 10 realisations of the estimated spectra of LoCapE overlaid on the magnitude DFT spectrum. Since we are only interested in the peak separation, we show the spectra with the magnitude normalised. It can be clearly seen that for both regions, the closely spaced peaks are not separated in the DFT but are clearly resolved by LoCapE and the energy of the components are more concentrated near the true frequencies.

3.2. Experimental Data Analysis

In order to further demonstrate the capacity of LoCapE for resolving closely spaced peaks in NMR spectrum, we applied the algorithm to an experimental ^{1}H NMR dataset of codeine in

solvent deuteriochloroform ($CDCl_3$). The FID is of length $16,384$. For this dataset, we applied LoCapE in five regions of interest and resolve the heavily overlapping peaks, so as to extract the coupling information that cannot be revealed by the DFT. In keeping with common practice in NMR, we compare the experimental results with the real part of the DFT of the signal with all the initial phases removed. The phase removal task is done using the phase correction function in the Bruker Topspin NMR processing software[1]. Although no coupling information of codeine is presented in the literature, as codeine as an opiate derivative shares a very similar structure to morphine, we use the coupling information of morphine [27] [28] [29] as a reference to support our deductions. In this test, according to the characteristic of proton datasets [30], the damping factor grid of the LoCapE is selected to be $\mathbf{\Gamma} = [0.0002, 0.0012]$. For comparison purposes, we also included the results of the original Capon estimator with $L = N/2 + 1$ (so $M = N/2$), which achieves the highest resolution.

Applying the algorithm to the selected regions of $\mathbf{f}_1 = [1.86, 1.94]$ (ppm) and $\mathbf{f}_2 = [2.56, 2.64]$ (ppm), the peaks in region $\mathbf{f}_1$ and $\mathbf{f}_2$ provide coupling information of protons $H_{15(\text{eq})}$ and $H_{16(\text{eq})}$ respectively[2] [32]. From [27] we know that $H_{15(\text{eq})}$ is coupled with protons $H_{15(\text{ax})}$, $H_{16(\text{ax})}$ and $H_{16(\text{eq})}$ which results in region $\mathbf{f}_1$ a doublet of doublet of doublet. Besides, proton $H_{16(\text{eq})}$ is coupled with protons $H_{16(\text{ax})}$, $H_{15(\text{ax})}$, $H_{15(\text{eq})}$ and H_9 [27] and should appear as a doublet of doublet of doublet of doublet in region $\mathbf{f}_2$. In these two regions, LoCapE was performed by setting the smoothing length to be $L = \lfloor N/3 \rfloor$ and the size of the localised region to be $r = 3$. We can find from Figure 9 that LoCapE can resolve the doublet of doublet of doublet in region $\mathbf{f}_1$, while Capon detected various spurious peaks due to the trade-off between accuracy and resolution, and DFT mis-detected the doublet with the smallest coupling constant. For region $\mathbf{f}_2$, only a doublet of doublet can be clearly observed from the DFT (which only shows the coupling information of $H_{16(\text{eq})} - H_{16(\text{ax})}$ and $H_{16(\text{eq})} - H_{15(\text{ax})}$), whereas LoCapE is able to give an extra doublet corresponded to the coupling of $H_{16(\text{eq})}$ and $H_{15(\text{eq})}$ which can be hardly observed through the DFT. Also notice that the rightmost peak of LoCapE spectral estimate is clearly a doublet, which reveals the coupling of $H_{16(\text{eq})}$ and H_9 which has the smallest coupling constant.

[1] https://www.bruker.com/products/mr/nmr/nmr-software/software/topspin/overview.html.

[2] $H_{(\text{eq})}$ and $H_{(\text{ax})}$ denote respectively the equatorial and axial protons associated with the same carbon [27, 31].

Then LoCapE was applied to the interested regions of $\mathbf{f}_3 = [2.27, 2.36]$ (ppm), $\mathbf{f}_4 = [3.00, 3.08]$ (ppm) and $\mathbf{f}_5 = [6.57, 6.61]$ (ppm), which contain peaks corresponding to proton $H_{10(\alpha)}$, $H_{10(\beta)}$ and H_1 respectively [3] [32]. Particularly, apart from the coupling with H_2, proton H_1 is also equivalently coupled with $H_{10(\alpha)}$ and $H_{10(\beta)}$ with a very small coupling constant of around 1 Hz [28] [27]. But this coupling can hardly be observed from the DFT in region $\mathbf{f}_5$, and is even not observable at $\mathbf{f}_3$ and $\mathbf{f}_4$. LoCapE was performed by using a smoothing length $L = \lfloor N/6 \rfloor$, with the size of the localised region remained as $r = 3$. From Figure 10 we can find that the coupling between protons H_1 and H_{10} is clearly indicated by LoCapE. LoCapE shows three peaks in each bulk in region $\mathbf{f}_5$, implying respectively the coupling information of $H_1 - H_2$, $H_1 - H_{10(\alpha)}$ and $H_1 - H_{10(\beta)}$ with the latter two close to equivalent. At the same time, a doublet of doublet of doublet in region $\mathbf{f}_3$ can be found, indicating the coupling information of $H_{10(\alpha)} - H_{10(\beta)}$, $H_{10(\alpha)} - H_9$ and $H_{10(\alpha)} - H_1$ accordingly [28]. In terms of region $\mathbf{f}_4$, the estimate of LoCapE also shows a doublet of doublet, indicating the coupling information of $H_{10(\beta)} - H_{10(\alpha)}$ and $H_{10(\beta)} - H_1$. Capon, on the other hand, is biased and has a lot of false alarms in these regions.

We tabulate in Table 2 the estimated coupling constants in all five regions obtained by LoCapE compared with the corresponding coupling information of morphine provided in literature [27], where we can find that the coupling constants are almost consistent. The reliability of LoCapE on resolving closely spaced peaks in NMR signals is therefore verified.

Finally, in order to demonstrate the repeatability of the experimental spectral estimate, in Figures 11 and 12 we show the performance of LoCapE on the same regions of another codeine sample with 32,768 time domain complex data points. To process this data, $r = 9$ and $L = \lfloor N/2 \rfloor$ are used in regions $\mathbf{f}_1$ and $\mathbf{f}_3$, while $r = 5$ and $L = \lfloor N/3 \rfloor$ are used in regions $\mathbf{f}_2, \mathbf{f}_4$ and $\mathbf{f}_5$. We can find from the results that LoCapE is still capable of resolving the overlapped peaks thus retrieving the corresponding coupling constants.

[3] H_α and H_β denote two equivalent protons associated with the same carbon [27, 31].

4. Conclusion

In this paper, we have presented the Localised Capon Estimator (LoCapE) for resolving closely spaced peaks in NMR spectrum. The algorithm is based on designing an adaptive filter bank that minimises the power of the output signal and the resulting spectrum estimate can achieve very high resolution by requiring no *a priori* information of the number of components. The presented algorithm can be efficiently implemented and it is capable to work as "zoom in" operator for detecting overlapped components in regions of interest in the DFT spectrum in rapid NMR analysis. The superiority of LoCapE on component detection and separation is confirmed by applications on both simulated and actual proton NMR signals.

Appendix: Efficient Implementation

From the above context we find that LoCapE requires the inversion of much smaller matrices than the original versions ($r \ll M$ and $r \ll L$). This significantly reduces the computational cost per frequency bin and it remains much smaller than the efficient implementations of the original versions [33, 34] for a reasonable number of bins. However, as the number of bins to be calculated increases, especially when calculating a dense grid, direct implementation of the localised versions can become burdensome. This is mainly caused by the brute force calculation of $\mathbf{F}^H\mathbf{X}$, which has a computational cost of $O(n_\eta n_F ML)$ ($O(Ln_\eta N_f \log N_f)$ for calculating the whole spectrum). Nevertheless, as is presented in the following, the localised algorithm can be efficiently implemented and the computational cost for computing each bin can be significantly reduced.

We now present the steps for efficiently calculating the estimation at every single frequency bin of interest f and every single damping factor bin η and show the necessary multiplications at each step. After the signal Hankel matrices are constructed, we first use the brute force implementation of Fourier transform to the first column of $\mathbf{X}$ and $\tilde{\mathbf{X}}$ to find the first column of $\bar{\mathbf{X}}$ and $\bar{\tilde{\mathbf{X}}}$. Denoting $\bar{\mathbf{X}} = [\mathbf{y}_1, \mathbf{y}_2, \ldots, \mathbf{y}_L]$, $\bar{\tilde{\mathbf{X}}} = [\tilde{\mathbf{y}}_1, \tilde{\mathbf{y}}_2, \ldots, \tilde{\mathbf{y}}_L]$ we have:

$$\mathbf{y}_1 = \bar{\mathbf{F}}^H\mathbf{x}_1 \quad \text{and} \quad \tilde{\mathbf{y}}_1 = \bar{\mathbf{F}}^H\tilde{\mathbf{x}}_1 \tag{19}$$

where $\bar{\mathbf{F}}$ is given by Eq. (13). To calculate Eq. (19) we need $2rM$ multiplications. Utilising the

special structure of Hankel matrices, we can then obtain the l^{th} column of $\bar{\mathbf{X}}$ by:

$$\mathbf{y}_l = [\mathbf{y}_{l-1} - x(l-1)] \cdot \mathbf{v} + x(l+M)\mathbf{u}, \tag{20}$$

where

$$\mathbf{v} = \left[e^{j2\pi(f-\frac{pq}{N_f})}, \ldots, e^{j2\pi(f-\frac{q}{N_f})}, e^{j2\pi f}, e^{j2\pi(f+\frac{q}{N_f})}, \ldots, e^{j2\pi(f+\frac{pq}{N_f})} \right]^T, \tag{21}$$

and

$$\mathbf{u} = \left[e^{j2\pi(f-\frac{pq}{N_f})(M-1)}, \ldots, e^{j2\pi(f-\frac{q}{N_f})(M-1)}, e^{j2\pi f(M-1)}, e^{j2\pi(f+\frac{q}{N_f})(M-1)}, \ldots, e^{j2\pi(f+\frac{pq}{N_f})(M-1)} \right]^T. \tag{22}$$

Note that "$\cdot$" is the point-wise multiplication of two vectors. This requires $2r$ multiplications. The l^{th} of column of $\bar{\tilde{\mathbf{X}}}$ can be similarly obtained by:

$$\begin{aligned} \tilde{\mathbf{y}}_l &= [\tilde{\mathbf{y}}_{l-1} - \tilde{x}(l-1)] \cdot \mathbf{v} + \tilde{x}(l+M)\mathbf{u} \\ &= [\tilde{\mathbf{y}}_{l-1} - x^*(N-l)] \cdot \mathbf{v} + x^*(N-l-M-1)\mathbf{u}. \end{aligned} \tag{23}$$

As a result, all the other columns of $\bar{\mathbf{X}}$ and $\bar{\tilde{\mathbf{X}}}$ can be efficiently calculated only using $\mathbf{y}_1$ and $\tilde{\mathbf{y}}_1$ and the total computational cost is $4r(L-1)$ multiplications.

After the calculation of $\bar{\mathbf{X}}$ and $\bar{\tilde{\mathbf{X}}}$, the inverse of the Fourier transformed localised autocorrelation matrix $\bar{\mathbf{R}}^{-1}$ and the computation of $\bar{\mathbf{X}}\mathbf{s}_L^*(f)$ are then obtained by direct multiplication, which need $2r^2L + r^3 + rL$ multiplications. Finally calculating Eq. (11) requires another $r^2 + 2r$ multiplications and one division.

Summing up the required multiplications yields the total computational cost for the estimation of one bin to be:

$$\begin{aligned} \Omega &= 2rM + 4r(L-1) + 2r^2L + r^3 + rL + r^2 + 2r \\ &\approx r[2M + (5+2r)L] \\ &\sim O(N). \end{aligned} \tag{24}$$

Here we also use the facts $r \ll M$ and $r \ll L$. Obviously, the cost for estimating $n_\eta n_f$ bins is only $\Omega \sim O(n_\eta n_f N)$ and the computational cost is now significantly reduced.

References

[1] R.S. Macomber, *A complete introduction to modern NMR spectroscopy*, Wiley-Interscience publication. Wiley, 1998.

[2] J.K. Nicholson, J. Connelly, J.C. Lindon, and E. Holmes, "Metabonomics: A platform for studying drug toxicity and gene function," *Nature Reviews Drug Discovery*, vol. 1, no. 2, pp. 153–161, 2002.

[3] P. Stoica, N. Sandgren, Y. Selen, L. Vanhamme, and S. Van Huffel, "Frequency-domain method based on the singular value decomposition for frequency-selective NMR spectroscopy," *Journal of Magnetic Resonance*, vol. 165, no. 1, pp. 80–88, 2003.

[4] R.O. Schmidt, "Multiple emitter location and signal parameter estimation," *IEEE Transactions on Antennas and Propagation*, vol. AP-34, no. 3, pp. 276–280, 1986.

[5] H. Barkhuijsen, R. de Beer, and D. van Ormondt, "Improved algorithm for noniterative time-domain model fitting to exponentially damped magnetic resonance signals," *Journal of Magnetic Resonance (1969)*, vol. 73, no. 3, pp. 553–557, 1987.

[6] R. Roy and T. Kailath, "ESPRIT - estimation of signal parameters via rotational invariance techniques," *IEEE Transactions on Acoustics, Speech, and Signal Processing*, vol. 37, no. 7, pp. 984–995, 1989.

[7] Y. Hua and T. K. Sarkar, "Matrix pencil method for estimating parameters of exponentially damped/undamped sinusoids in noise," *IEEE Transactions on Acoustics, Speech, and Signal Processing*, vol. 38, no. 5, pp. 814–824, 1990.

[8] Y.-Y. Lin, P. Hodgkinson, M. Ernst, and A. Pines, "A novel detection-estimation scheme for noisy NMR signals: Applications to delayed acquisition data," *Journal of Magnetic Resonance*, vol. 128, no. 1, pp. 30–41, 1997.

[9] H. Akaike, "A new look at the statistical model identification," *IEEE Transactions on Automatic Control*, vol. 19, no. 6, pp. 716–723, Dec 1974.

[10] J. Rissanen, "A universal prior for integers and estimation by minimum description length," *Annals of Statistics*, 1982.

[11] N. Sandgren, Y. Selen, P. Stoica, and J. Li, "Parametric methods for frequency-selective MR spectroscopy - a review," *Journal of Magnetic Resonance*, vol. 168, no. 2, pp. 259–272, 2004.

[12] J. Capon, "High-resolution frequency-wavenumber spectrum analysis," *Proceedings of the IEEE*, vol. 57, no. 8, pp. 1408 – 1418, 1969.

[13] J. Li and P. Stoica, "An adaptive filtering approach to spectral estimation and SAR imaging," *IEEE Transactions on Signal Processing*, vol. 44, no. 6, pp. 1469–1484, 1996.

[14] T. Yardibi, J. Li, P. Stoica, M. Xue, and A.B. Baggeroer, "Source localization and sensing: A nonparametric iterative adaptive approach based on weighted least squares," *IEEE Transactions on Aerospace and Electronic Systems*, vol. 46, no. 1, pp. 425–443, Jan 2010.

[15] P. Stoica and T. Sundin, "Nonparametric NMR spectroscopy," *Journal of Magnetic Resonance*, vol. 152, no. 1,

pp. 57–69, 2001.

[16] Y. Kopsinis, E. Aboutanios, D. A. Waters, and S. McLaughlin, "Time-frequency and advanced frequency estimation techniques for the investigation of bat echolocation calls," *The Journal of the Acoustical Society of America*, vol. 127, no. 2, pp. 1124–1134, 2010.

[17] M. F. Duarte and R. G. Baraniuk, "Spectral compressive sensing," *Applied and Computational Harmonic Analysis*, vol. 35, no. 1, pp. 111–129, 2013.

[18] L. C. Potter, E. Ertin, J. T. Parker, and M. Cetin, "Sparsity and compressed sensing in radar imaging," *Proceedings of the IEEE*, vol. 98, no. 6, pp. 1006–1020, June 2010.

[19] X. X. Zhu and R. Bamler, "Super-resolution power and robustness of compressive sensing for spectral estimation with application to spaceborne tomographic SAR," *IEEE Transactions on Geoscience and Remote Sensing*, vol. 50, no. 1, pp. 247–258, Jan 2012.

[20] A. S. Stern and J. C. Hoch, "A new approach to compressed sensing for NMR," *Magnetic Resonance in Chemistry*, vol. 53, no. 11, pp. 908–912, 2015.

[21] J.-B. Poullet, D.M. Sima, A.W. Simonetti, B. De Neuter, L. Vanhamme, P. Lemmerling, and S. Van Huffel, "An automated quantification of short echo time MRS spectra in an open source software environment: AQSES," *NMR in Biomedicine*, vol. 20, no. 5, pp. 493–504, 2007.

[22] S. Ye and E. Aboutanios, "Localised Capon spectral estimator with application to the processing of NMR signals," in *EUSIPCO, European Signal Processing Conference - Proceedings*, 2013.

[23] A. Jakobsson and P. Stoica, "Combining Capon and APES for estimation of spectral lines," *Circuits, Systems, and Signal Processing*, vol. 19, no. 2, pp. 159–169, 2000.

[24] H. Li, J. Li, and P. Stoica, "Performance analysis of forward-backward matched-filterbank spectral estimators," *IEEE Transactions on Signal Processing*, vol. 46, no. 7, pp. 1954–1966, 1998.

[25] A. Jakobsson and P. Stoica, "Combining Capon and APES for estimation of spectral lines," *Circuits, Systems, and Signal Processing*, vol. 19, no. 2, pp. 159–169, 2000.

[26] Y. Yao and S. M. Pandit, "Cramer-Rao lower bounds for a damped sinusoidal process," *IEEE Transactions on Signal Processing*, vol. 43, no. 4, pp. 878–885, 1995.

[27] G. A. Neville, I. Ekiel, and I. C. P. Smith, "High-resolution proton magnetic resonance spectra of morphine and its three O-acetyl derivatives," *Magnetic Resonance in Chemistry*, vol. 25, no. 1, pp. 31–35, 1987.

[28] J. A. Glasel and H. W. Reiher, "Very high frequency proton NMR studies of the conformations of opiate agonists and antagonists," *Magnetic Resonance in Chemistry*, vol. 23, no. 4, pp. 236–242, 1985.

[29] S. Luong, R. Shimmon, J. Hook, and S. Fu, "2-Nitro-6-monoacetylmorphine: potential marker for monitoring the presence of 6-monoacetylmorphine in urine adulterated with potassium nitrite," *Analytical and Bioanalytical Chemistry*, vol. 403, no. 7, pp. 2057–2063, 2012.

[30] S. Ye and E. Aboutanios, "Efficient peak extraction of proton NMR spectroscopy using lineshape adaptation,"

in *ICASSP, IEEE International Conference on Acoustics, Speech and Signal Processing - Proceedings*, 2014.

[31] E.L. Eliel, *Conformational Analysis*, Interscience Publishers, 1965.

[32] M. M. Nair, G. E. Jackson, and W. E. Campbell, "Structural assignment of the opium alkaloid, codeine via 2D NMR techniques," *Spectroscopy Letters*, vol. 30, no. 3, pp. 497–505, 1997.

[33] G.-O. Glentis, "A fast algorithm for APES and Capon spectral estimation," *IEEE Transactions on Signal Processing*, vol. 56, no. 9, pp. 4207–4220, 2008.

[34] E.G. Larsson and P. Stoica, "Fast implementation of two-dimensional APES and Capon spectral estimators," *Multidimensional Systems and Signal Processing*, vol. 13, no. 1, pp. 35–53, 2002.

Table 1: Parameters of the simulated NMR signal.

Component No.	Amplitude	Frequency	Damping ($\times 10^{-2}$)
1	5	0.2	2
2	1	0.5	1
3	0.8	0.502	1
4	0.3	0.695	1.8
5	1	0.7	1.5
6	0.5	0.703	1.5

Table 2: Estimated coupling constants in Hz for protons in the five selected regions of codeine compared with the coupling constants for the corresponding opiate protons of morphine presented in [27].

System	Codeine (in $CDCl_3$)	Morphine (in $CDCl_3$)	Morphine (in CD_3OD)
$H_{15(eq)}$ - $H_{15(ax)}$	12.65	12.4	12.7
$H_{15(eq)}$ - $H_{16(eq)}$	1.85	-	1.7
$H_{15(eq)}$ - $H_{16(ax)}$	3.85	3.6	3.6
$H_{16(eq)}$ - $H_{16(ax)}$	12.1	12.1	12.3
$H_{16(eq)}$ - $H_{15(ax)}$	5.0	5.0	5.1
$H_{16(eq)}$ - H_9	1.0	-	0.8
H_1 - H_2	7.9	8.1	8.1
H_1 - H_{10}	1.19	-	0.95
$H_{10(\beta)}$ - $H_{10(\alpha)}$	18.5	18.5	18.6
$H_{10(\alpha)}$ - H_9	6.25	6.1	6.3

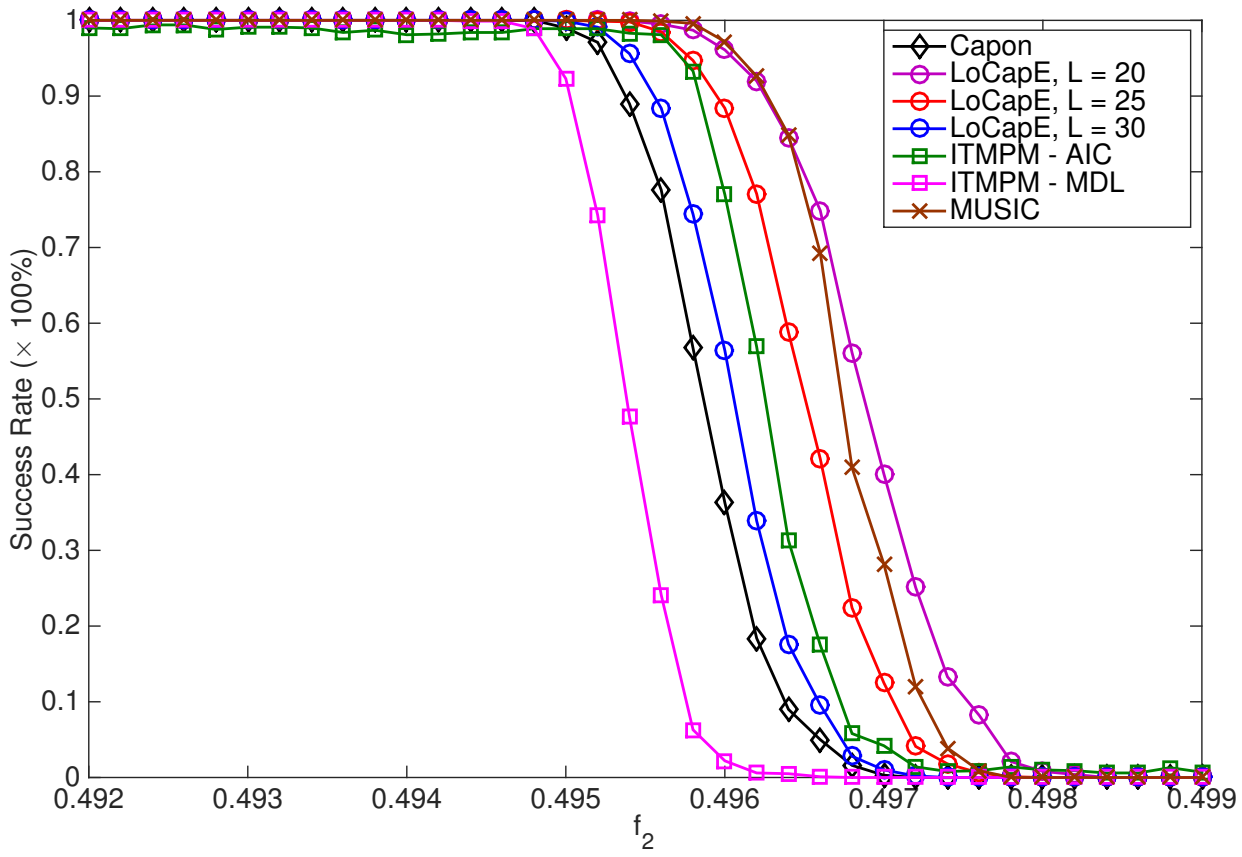

Figure 1: Evaluation of the ability to resolve two closely spaced undamped peaks of LoCapE and other algorithms versus the distance between the peaks. SNR = 25dB, $f_1 = 0.5$ and θ were randomly chosen. 1,000 Monte Carlo runs were used.

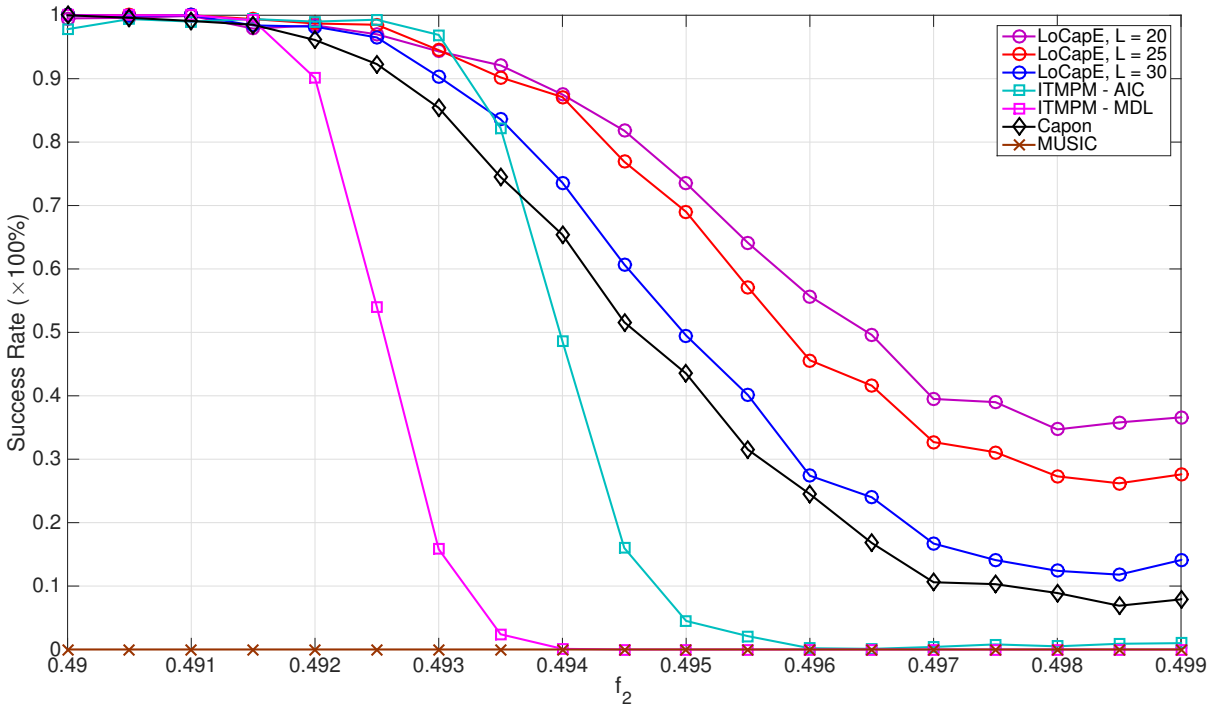

Figure 2: Evaluation of the ability to resolve two closely spaced damped peaks of LoCapE and other algorithms versus the distance between the peaks. SNR = 25dB, $f_1 = 0.5$, $\eta = 0.03$ and θ were randomly chosen. 1,000 Monte Carlo runs were used.

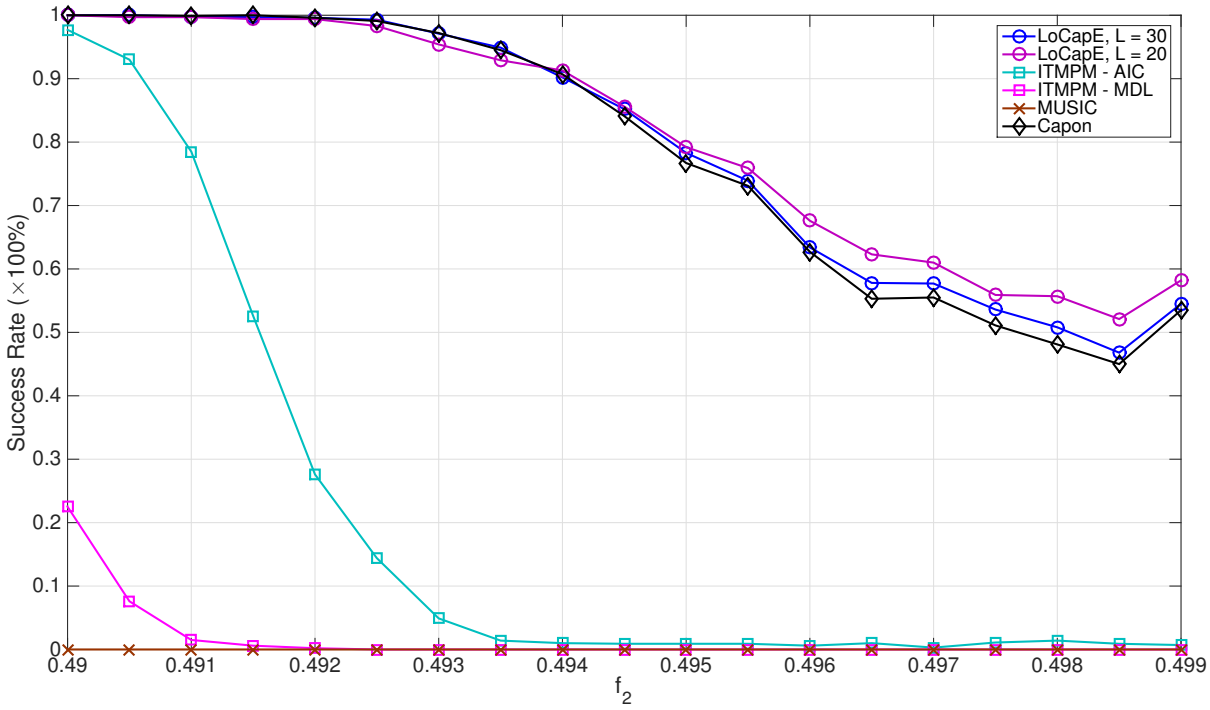

Figure 3: Evaluation of the ability to resolve two closely spaced undamped peaks of LoCapE and other algorithms versus the distance between the peaks. SNR = 25dB, $f_1 = 0.5$, $\eta = 0.05$ and θ were randomly chosen. 1,000 Monte Carlo runs were used.

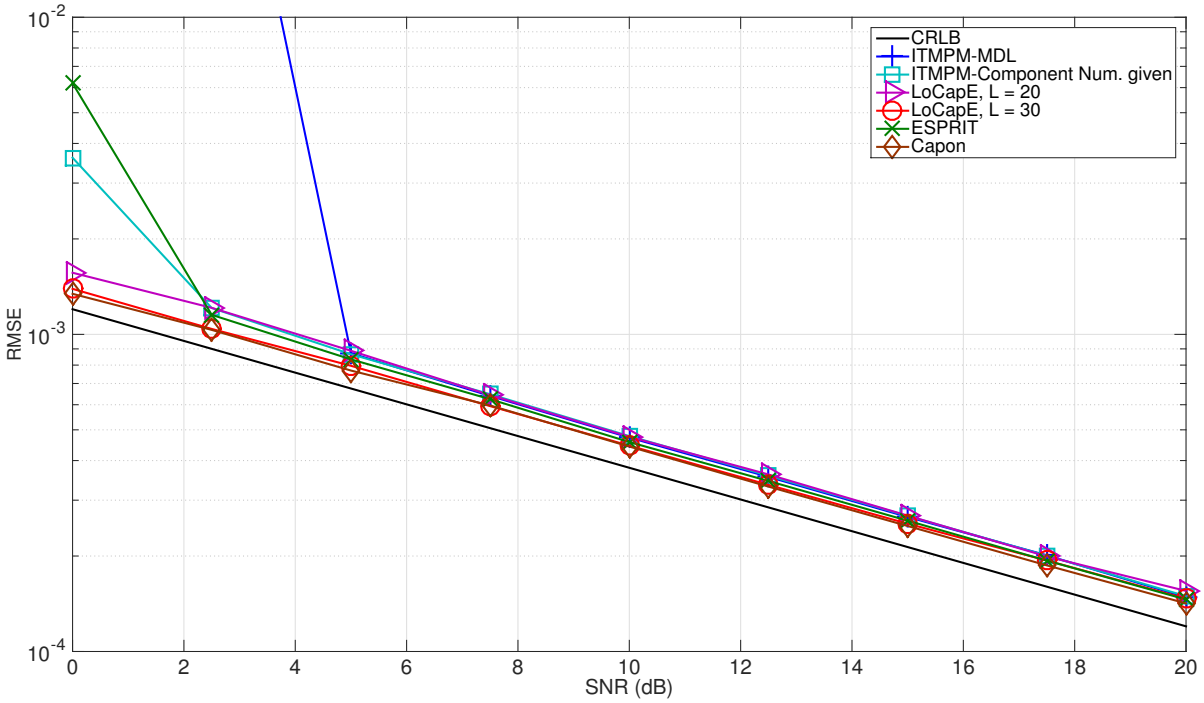

Figure 4: Evaluation of the frequency estimation accuracy obtained by LoCapE and other algorithms versus SNR. $f_1 = 0.5$, $f_2 = 0.48$, $\eta = 0$ and θ were randomly chosen in each run. 5,000 Monte Carlo runs were used.

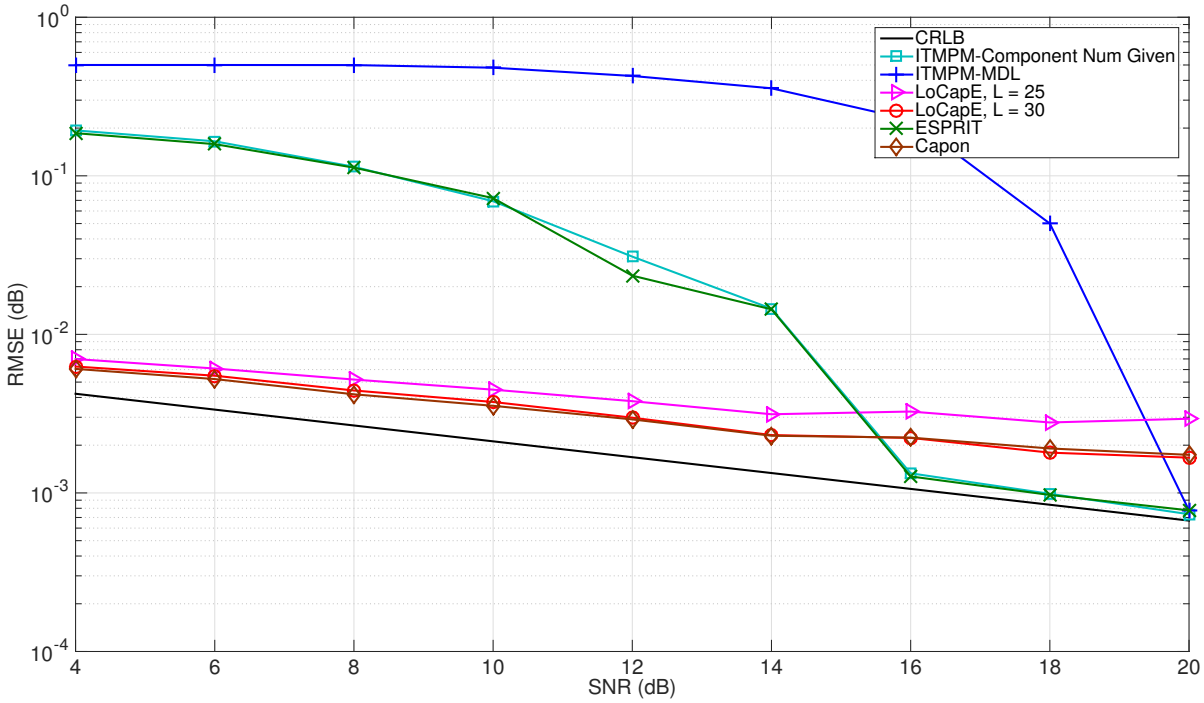

Figure 5: Evaluation of the frequency estimation accuracy obtained by LoCapE and other algorithms versus SNR. $f_1 = 0.5$, $f_2 = 0.48$, $\eta = 0.05$ and θ were randomly chosen in each run. 5,000 Monte Carlo runs were used.

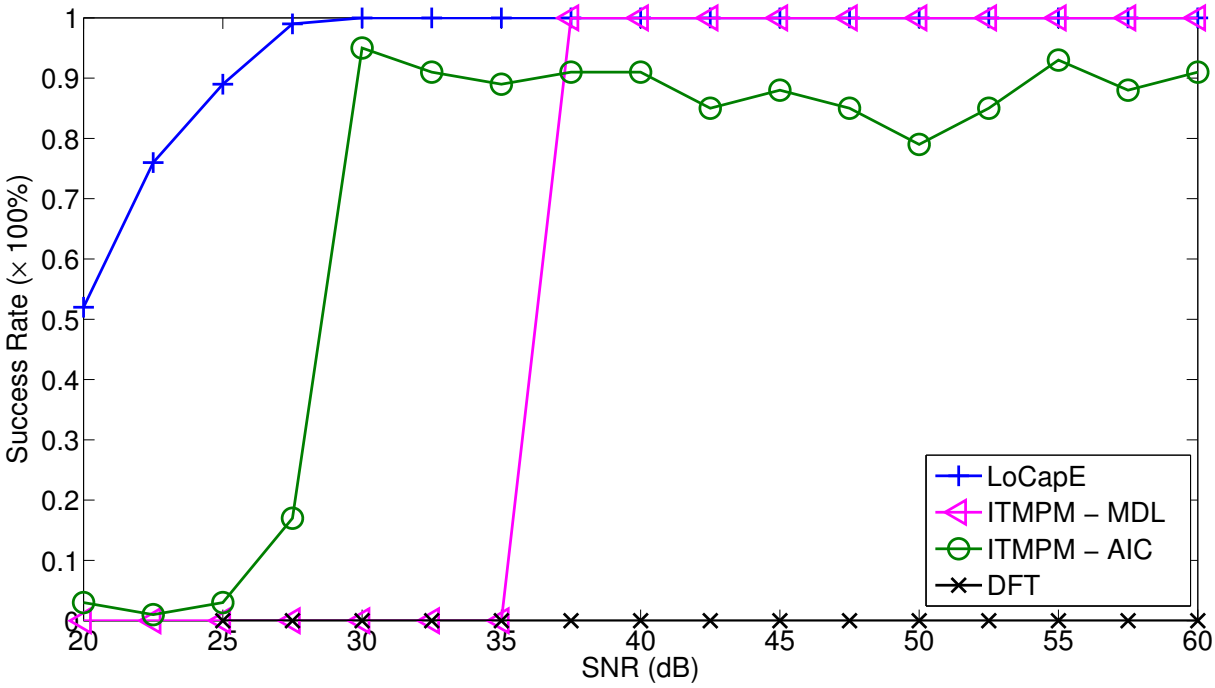

Figure 6: The success rates of LoCapE, ITMPM and DFT in resolving components 2-6 in the simulated NMR signal versus SNR. 100 Monte Carlo runs were used.

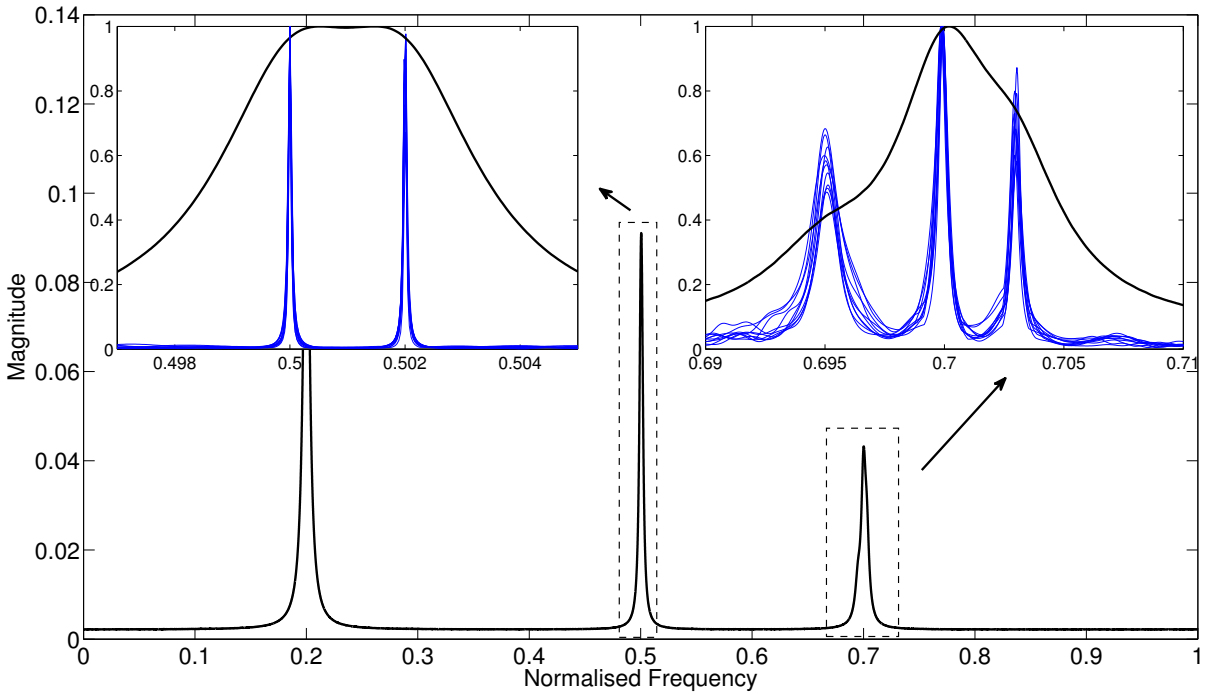

Figure 7: Evaluation of the performance of LoCapE in resolving closely spaced peaks in the simulated NMR spectrum with SNR = 60dB. 10 realisations of the LoCapE result are shown in each region. Black: Magnitude DFT spectrum; Blue: LoCapE.

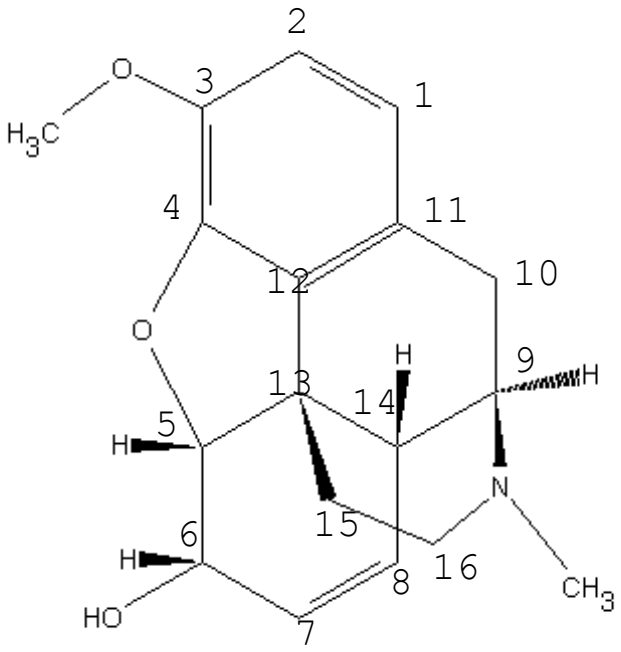

Figure 8: Chemical structure of codeine.

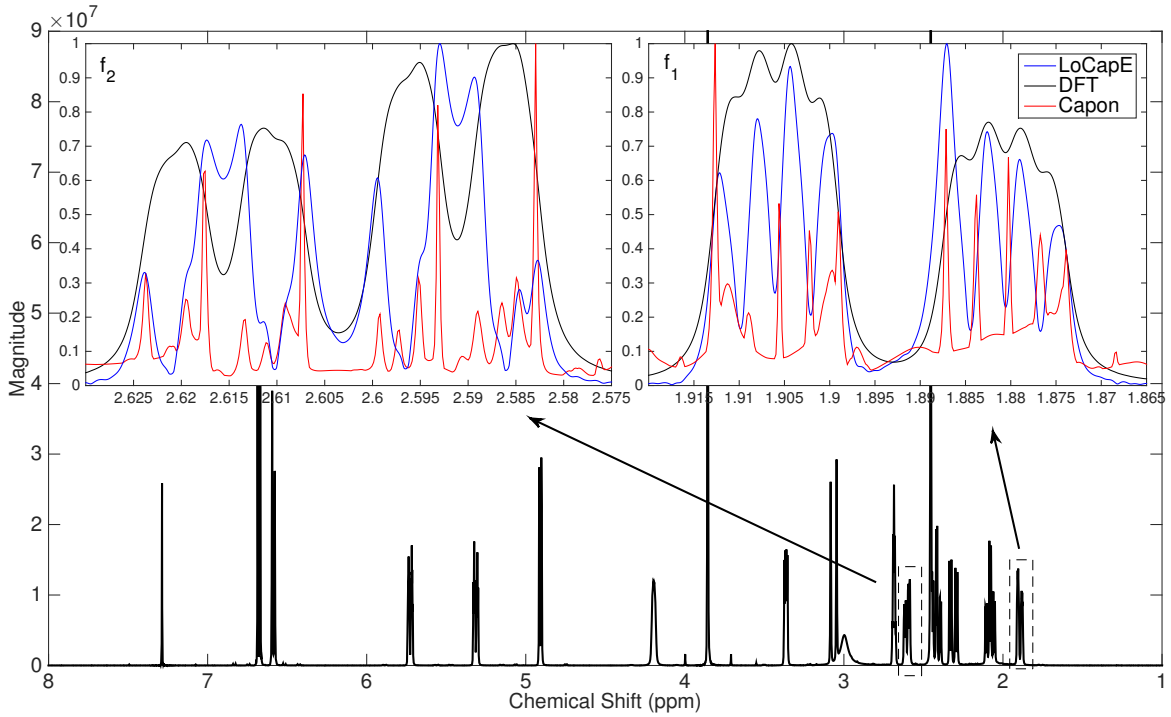

Figure 9: Evaluation of the performance of LoCapE on separating the peaks in regions $\mathbf{f}_1$ and $\mathbf{f}_2$ in codeine. Black: Real part of DFT; Blue: LoCapE; Red: Capon.

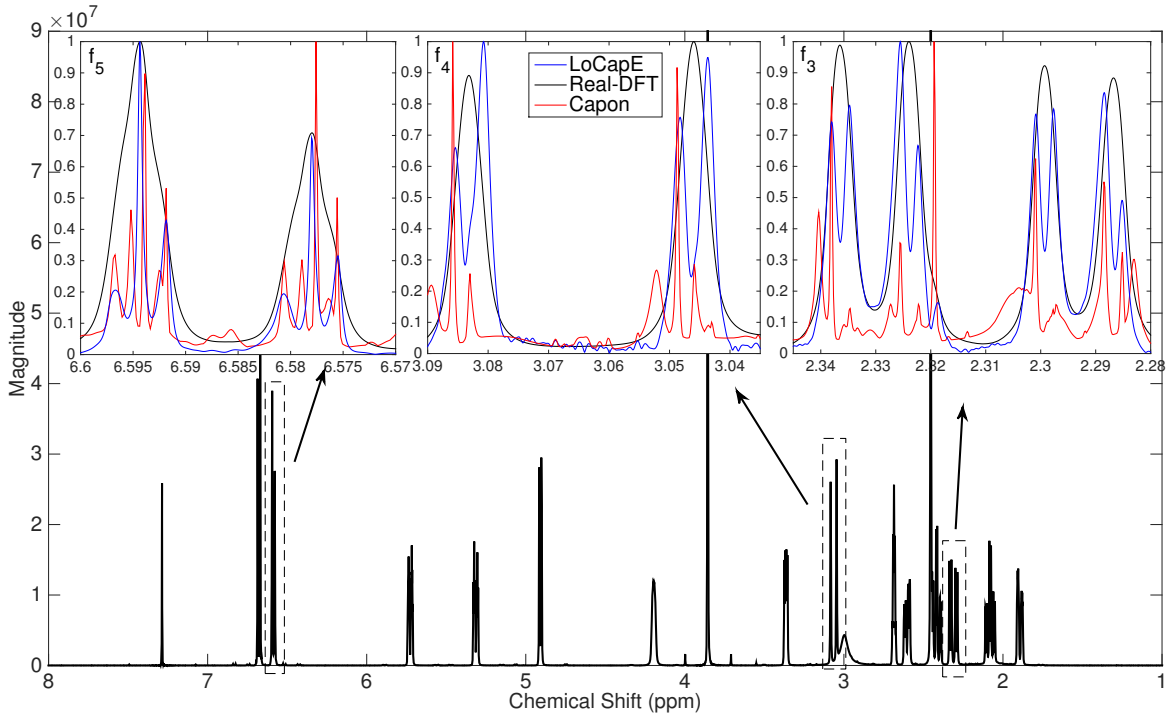

Figure 10: Evaluation of the performance of LoCapE on separating the peaks in regions $\mathbf{f}_3$, $\mathbf{f}_4$ and $\mathbf{f}_5$ in codeine. Black: Real part of DFT; Blue: LoCapE; Red: Capon.

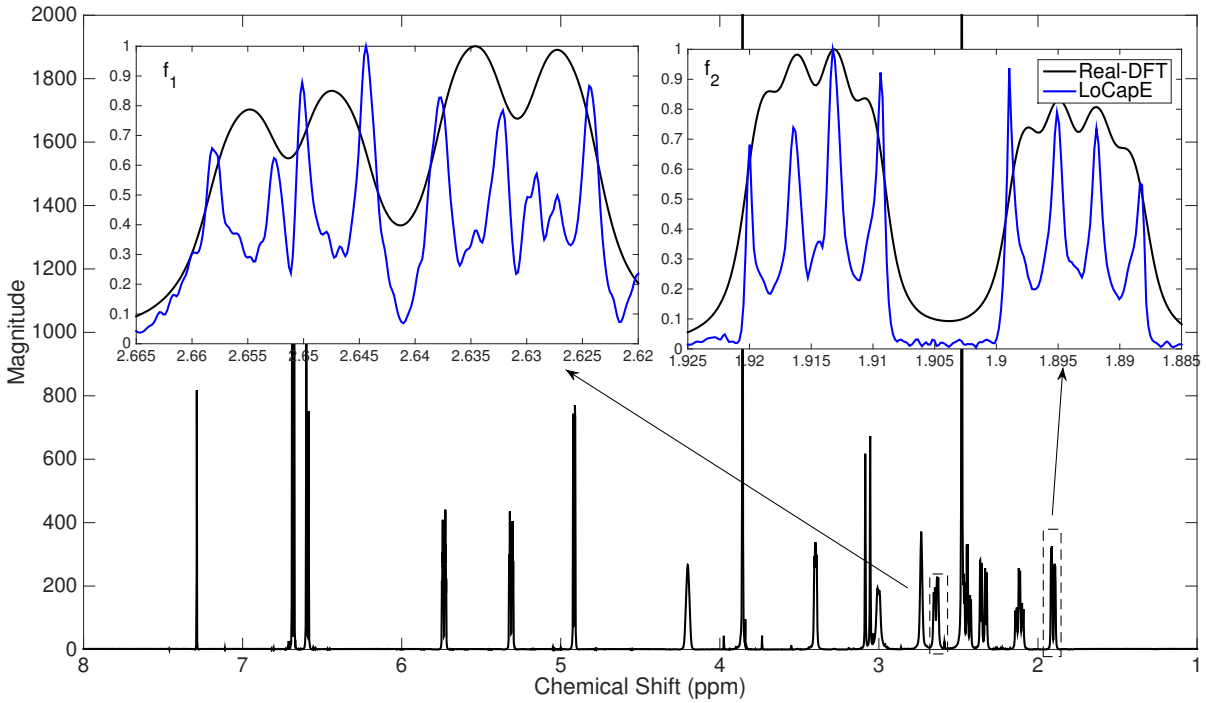

Figure 11: Evaluation of the performance of LoCapE on separating the peaks in regions $\mathbf{f}_1$ and $\mathbf{f}_2$ in another codeine sample. Black: Real part of DFT; Blue: LoCapE.

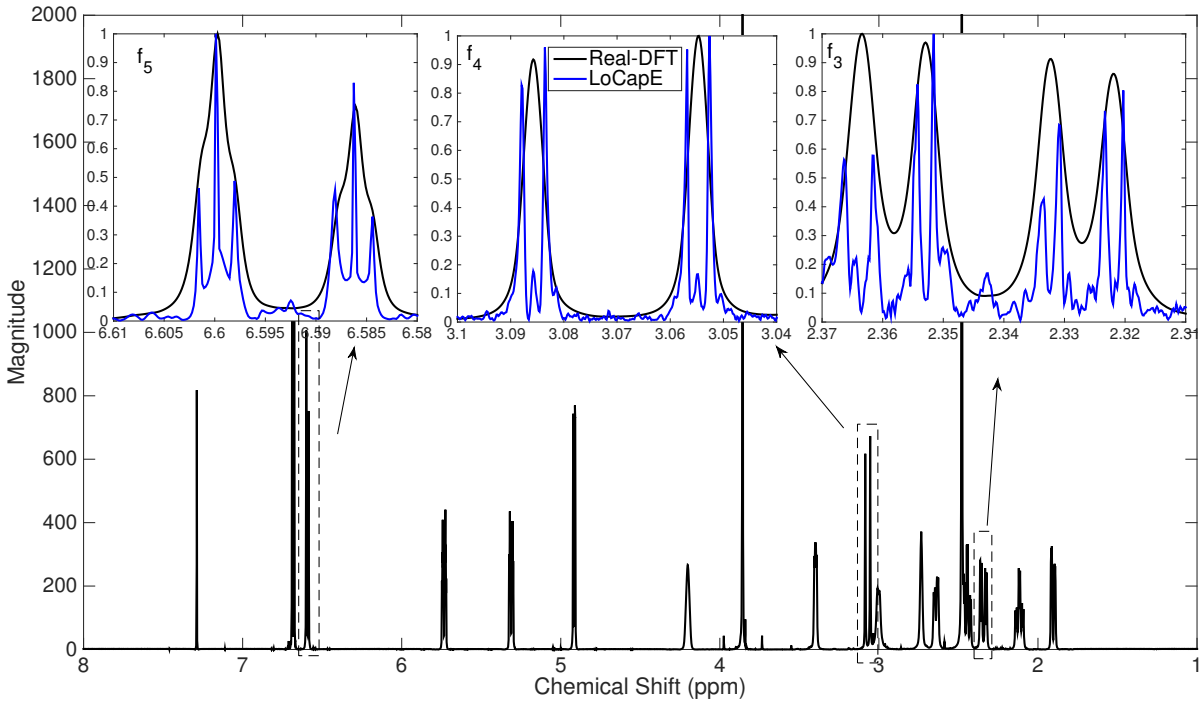

Figure 12: Evaluation of the performance of LoCapE on separating the peaks in regions $\mathbf{f}_3$, $\mathbf{f}_4$ and $\mathbf{f}_5$ in another codeine sample. Black: Real part of DFT; Blue: LoCapE.